DOI: https://doi.org/10.62985/j.huit_ojs.vol26.no2E.425

A SINGLE-STAGE DIFFERENTIAL BOOST DC-AC INVERTER WITH SIMPLIFIED CONTROL FOR ON-BOARD ELECTRIC VEHICLE CHARGERS

Trong-Tri Nguyen, Quoc-Anh Le, Hoang-Vu Nguyen*

Faculty of Electrical Engineering, Can Tho University, Can Tho, VietNam

*Email: *hoangvu@ctu.edu.vn*

Received: 22 December 2025; Revised:18 March 2026; Accepted: 7 April 2026

ABSTRACT

This paper proposes a single-stage DC-AC boost inverter topology for low-voltage DC sources, addressing the limitations of conventional two-stage converters that utilize separate boost and inversion stages, which result in increased complexity, cost, and power losses. The proposed topology achieves simultaneous DC voltage boosting and AC inversion within a single power conversion stage. Detailed analysis of the operating principles and switching states is presented, leading to the development of a comprehensive boost inverter model that incorporates capacitor voltage and inductor current controllers. Performance validation is conducted through simulations under varying input voltage and load conditions, demonstrating robust voltage boosting capability and stable sinusoidal output. Additionally, a low-power hardware prototype is implemented using a TMS320F28379D microcontroller for digital control. Experimental results confirm the inverter's capabilities in voltage boosting, reliable inversion, stable output regulation, and generation of sinusoidal waveforms with low total harmonic distortion.

Keywords: DC–AC conversion, Differential boost inverter, Output voltage control, Single-phase inverter, TMS320F28379D.

1. INTRODUCTION

Single-phase inverters are widely employed in various applications including uninterruptible power supplies, battery-based energy storage systems, and distributed renewable energy sources [1]. Their primary function is to convert DC voltage into AC voltage with a near-sinusoidal waveform while maintaining stable amplitude and frequency according to load requirements. Among various topologies, the H-bridge inverter is commonly adopted due to its simple structure, straightforward implementation, and high reliability.

However, a fundamental limitation of the conventional H-bridge inverter is its inability to provide voltage boosting, as the AC output voltage amplitude is inherently constrained by the DC input voltage level. To address this limitation, a two-stage configuration combining a DC-DC boost converter followed by an inverter stage is typically employed [2]. While effective in achieving voltage gain, this approach introduces several drawbacks including increased component count, higher switching losses, larger system footprint, and reduced overall efficiency [3], thereby motivating the development of single-stage inverter topologies with integrated voltage-boosting capability.

One promising alternative is the differential boost inverter, which integrates both voltage boosting and DC-AC conversion into a single power stage through two symmetrically operated boost branches [4]. This topology offers advantages in terms of reduced component count and improved power density. However, output voltage regulation remains challenging due to the

inherent nonlinear characteristics of the boost converter and the critical requirement to maintain voltage balance between the two branches [5].

This paper presents a comprehensive output voltage control strategy for a single-phase differential boost inverter implemented on a TMS320F28379D digital signal processor. The proposed control approach is validated through closed-loop simulations and experimental tests, demonstrating the system's capability to generate stable sinusoidal AC voltage with amplitude exceeding the DC input voltage while maintaining low harmonic distortion and robust performance under varying operating conditions.

In previously reported differential boost inverter systems, the control strategy is typically based on a closed-loop structure combining voltage and current regulation. In contrast, this work adopts a simplified open-loop approach, where the duty cycle is directly derived from analytical relationships among the DC input voltage, desired RMS output voltage, and capacitor voltages, eliminating the need for feedback loops or PI controllers. This significantly reduces control complexity while maintaining acceptable output voltage quality under normal conditions, making the proposed method more suitable for low-power or laboratory-scale applications where simplicity, cost, and ease of implementation are important considerations.

2. THEORETICAL BASIS

2.1. Single-phase Boost Inverter Topology

The single-phase boost inverter investigated in this paper is based on a differential boost inverter topology, in which the DC voltage boosting function and AC voltage generation are integrated into a single power conversion stage. Compared with conventional two-stage inverter structures, this topology reduces the number of power components and simplifies the overall circuit. As a result, it is well suited for applications supplied by low-voltage DC sources.

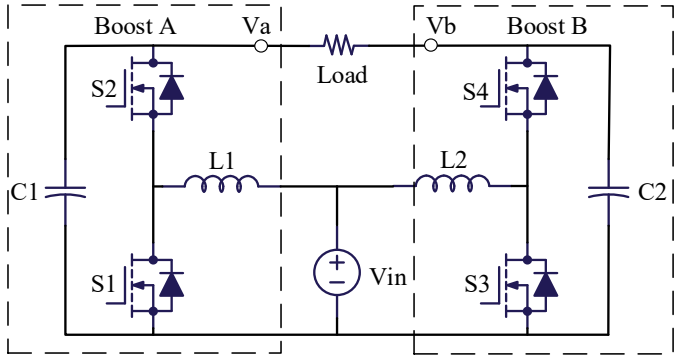

Fig. 1. Single-phase differential boost inverter topology.

Fig. 1 illustrates the schematic of the single-phase differential boost inverter topology considered in this study. The circuit consists of two symmetrical boost branches sharing a common DC input voltage V_{dc}. Each branch is composed of an inductor, power semiconductor switches, and an output capacitor, while the two capacitors are connected in series. With this differential configuration, the AC output voltage is not taken from an individual capacitor but is obtained from the voltage difference between the two capacitor voltages [6]. This voltage synthesis method allows the inverter to achieve an output voltage amplitude higher than the input DC voltage without an additional boost stage. This structural feature represents a key advantage of the proposed inverter topology.

2.2. Basic Operating Principle

The operating principle of the single-phase boost inverter can be explained by considering

each boost branch, where the inductor stores and transfers energy and the power switches control the charging and discharging process, similar to a conventional DC–DC boost converter. When a switch is turned on, the inductor is connected to the DC source and stores energy, while when the switch is turned off, the stored energy is transferred to the capacitor, increasing its voltage above the input level.

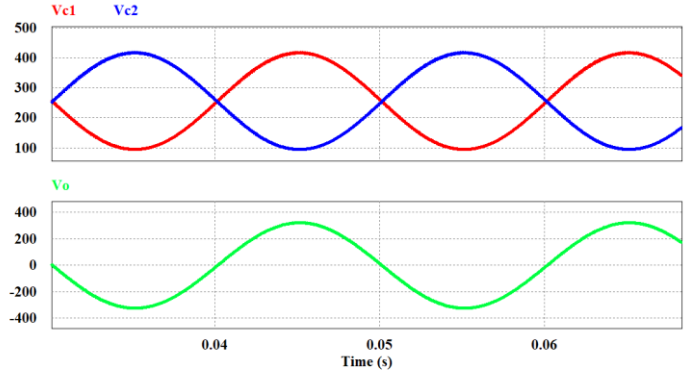

Fig. 2. Conceptual waveforms of capacitor voltages and output voltage.

As illustrated in Fig. 2, the two capacitor voltages contain AC components with opposite phases but similar DC average values, and their difference therefore produces a near-sinusoidal AC output voltage. The AC output voltage of the inverter is synthesized from the voltage difference between the two capacitor voltages of the boost branches and can be expressed as

$$V_o(t) = V_{c1}(t) - V_{c2}(t) \quad (1)$$

where $V_{c1}(t)$ and $V_{c2}(t)$ denote the capacitor voltages of the two boost branches, and $V_o(t)$ represents the inverter output voltage.

2.3. Switching States of The Single-Phase Boost Inverter

To further analyze the operation of the single-phase boost inverter, the circuit is examined through four fundamental switching states of the power switches in the two boost branches. Each switching state corresponds to a specific energy flow path between the DC source, inductors, capacitors, and the load. This switching-state analysis provides a clear understanding of the voltage boosting process and the differential voltage synthesis.

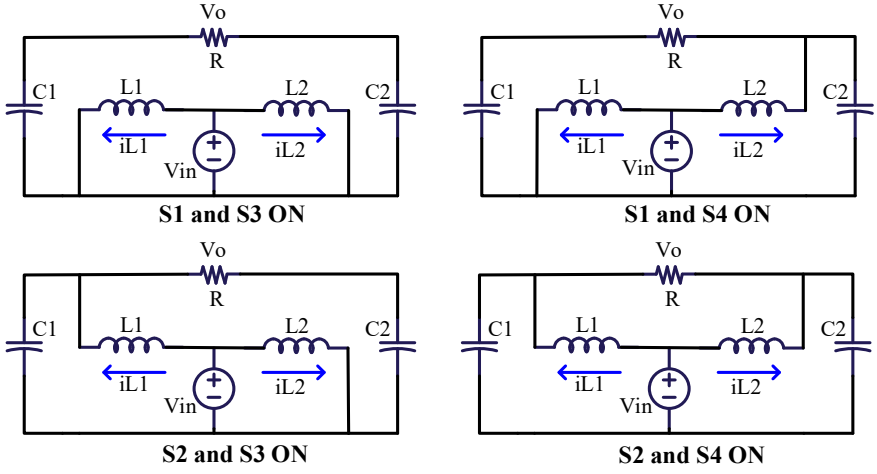

Fig. 3. Four different switching states for the boost inverter.

Fig. 3 illustrates the four fundamental switching states of the proposed single-phase

differential boost inverter within one switching period [7]. When S1 and S3 are turned on, both inductors store energy while the capacitors supply the load, resulting in an output voltage close to zero; in the remaining states, the two branches operate complementarily to generate positive or negative output voltage, and when S2 and S4 are on simultaneously, both inductors discharge to the capacitors, supporting voltage balancing and continuous AC output synthesis.

3. SYSTEM DESIGN AND CONTROL METHODS

3.1. Selection of Capacitors and Inductors

Table 1. Basic simulation and experimental parameters.

Parameter	Simulation	Experiment
Input DC voltage V_{in}	100 V	70 V
Output AC voltage V RMS	220 V	110 V
Output frequency f	50 Hz	50 Hz
Load R_{load}	40 Ω	40 Ω
Output power	1.2 kW	302 W
Inductors L_1, L_2	1 mH	
Capacitor C_1, C_2	150 μF	
Switching frequency f_{sw}	20 kHz	

In the simulation study, the boost inverter operates in a closed-loop configuration with a 100 V DC input to generate a 220 V RMS, 50 Hz output on a 40 Ω resistive load, allowing accurate evaluation of voltage regulation and tracking performance. In contrast, the experimental setup is implemented in open-loop mode with a reduced input voltage of 70 V, producing approximately 110 V RMS at 50 Hz to ensure safe operation of the hardware and measurement system. This configuration is sufficient to verify the voltage step-up capability, differential operation of the two boost branches, and the quality of the generated AC output waveform. The value of the inductor, output capacitor, and switching devices is guided by the power stage design recommendations provided in Texas Instruments application notes for converter [8]. Table 1 summarizes the basic parameters used in both the simulation and experimental setups.

To ensure stable output voltage and limit losses, the inductor ripple current is selected as 30% of the output current, giving:

$$\Delta I_L = (0.2\ to\ 0.4) \times I_{out(\max)} \times \frac{V_{out(\max)}}{V_{in}} \tag{2}$$

Once the allowable current ripple has been determined, the inductance is calculated using the expression:

$$L = \frac{V_{in} \times (V_{out} - V_{in})}{\Delta I_L \times f_s \times V_{out}} \tag{3}$$

To ensure that the DC voltage remains sufficiently smooth under rated operating conditions, the allowable peak to peak voltage ripple is restricted to $\Delta V_{out} = 1\%$.

Based on these requirements, the minimum output capacitance is determined using the standard boost capacitor sizing expression:

$$C_{out(\min)} = \frac{I_{out(\max)} \times D_{max}}{f_s \times \Delta V_{out}} \tag{4}$$

According to the current relation of a boost converter operating in CCM, the peak switch current is given by:

$$I_{SW(max)} = \frac{\Delta I_L}{2} + \frac{I_{out(max)}}{1-D} \tag{5}$$

In this design, a device with a continuous drain current of at least 20 A and a pulse current capability of at least 40 A is chosen.

The selection of power devices in the proposed converter is mainly determined by the voltage and current stresses imposed on the switching components. Specifically, the semiconductor devices must be capable of withstanding the maximum capacitor voltage as well as the peak inductor current under worst-case operating conditions. In addition, factors such as switching frequency, conduction losses, and thermal constraints must be carefully considered to ensure reliable and efficient operation. For the low-power prototype presented in this study, MOSFETs with moderate voltage and current ratings are sufficient to meet these requirements.

3.2. Control Method

Fig. 4 illustrates the closed-loop control structure used in the simulation model of the differential boost inverter. The controller is organized in two cascaded levels: outer capacitor voltage control loops and inner inductor current control loops. The final outputs of the controller are the duty cycles d_1 and d_2 for the two converter legs [9].

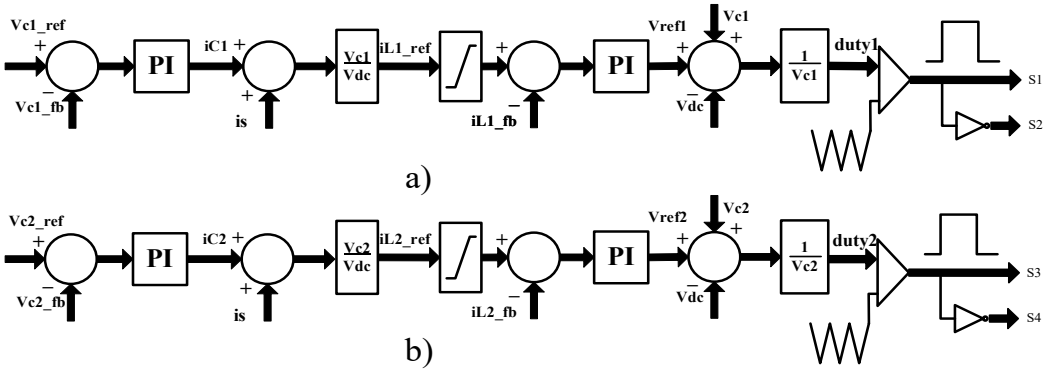

Fig. 4. Closed-loop control structure of the proposed differential boost inverter in simulation. (a) control loop for leg A (S1–S2). (b) control loop for leg B (S3–S4).

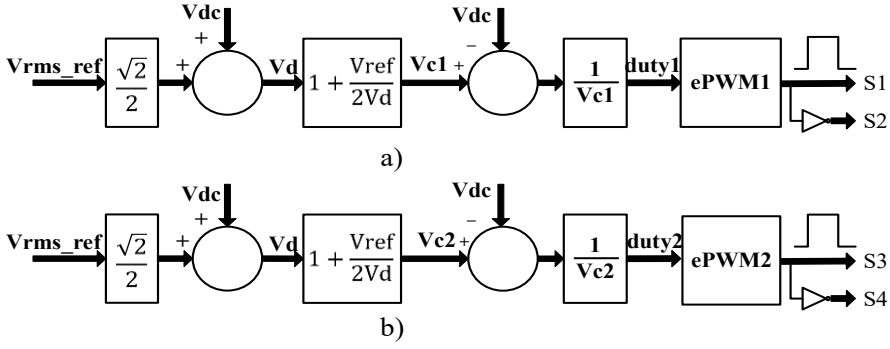

Fig. 5. Open-loop control algorithm implemented on the TMS320F28379D DSP. (a) control path left branch (S1–S2). (b) control path for right branch (S3–S4).

The open-loop control strategy implemented on the TMS320F28379D DSP is illustrated in Fig. 5. Fig. 5(a) shows the control flow for the upper boost leg (S1–S2), while Fig. 5(b) presents the corresponding structure for the lower boost leg (S3–S4). Both branches receive the

same reference RMS voltage $V_{rms_{ref}}$ and the input DC voltage V_{dc}, and compute the duty cycles directly without using any PI controllers or feedback signals.

The first block, sine reference generation creates the desired output voltage waveform in the form of a 50 Hz sinusoid. Starting from the RMS setpoint V_{rms}, the peak value is obtained, and the reference is calculated as:

$$V_{ref}(t) = V_{rms}\sqrt{2}\sin(\omega t) \tag{6}$$

where $\omega = 2\pi \cdot 50$ rad/s. This signal represents the ideal differential output voltage that the inverter should produce.

The second block, offset voltage calculation determines the DC offset V_d around which the capacitor voltages will oscillate. The offset is chosen as

$$V_d = V_{dc} + 0.5\,V_{rms}\sqrt{2} \tag{7}$$

So that both capacitor voltages remain positive and there is sufficient headroom for modulation even when the sinusoidal component reaches its peak. Based on this offset, the Capacitor Voltage Reference block generates the reference voltages for the two DC capacitors:

$$V_{C1} = V_d + 0.5V_{ref}, \tag{8}$$

$$V_{C2} = V_d - 0.5V_{ref} \tag{9}$$

With this definition, the differential capacitor voltage satisfies $V_{C1} - V_{C2} = V_{ref}(t)$, ensuring that the inverter output follows the sinusoidal reference.

The duty computation block converts the capacitor voltage reference into a duty cycle using the inverse relation of an ideal boost converter,

$$duty1 = \frac{V_{C1} - V_{dc}}{V_{C1}}, \tag{10}$$

$$duty2 = \frac{V_{C2} - V_{dc}}{V_{C2}} \tag{11}$$

Applied separately to the left and right legs. Finally, the PWM generator (ePWM1/2) produce the gate signals for the power switches. In this way, the desired sinusoidal output is obtained directly from the analytical relations between V_{dc}, V_{rms}, the capacitor voltage references and the duty cycles, without any feedback or PI controllers.

4. SIMULATION RESULTS

The simulations were carried out in PSIM software to evaluate the operating characteristics of the proposed single-phase differential boost inverter under various operating conditions. The nominal DC input voltage was set to 100 V, while the reference AC output voltage was 220 V RMS at a frequency of 50 Hz. A purely resistive load was employed in all simulation scenarios.

4.1. Steady-State Performance

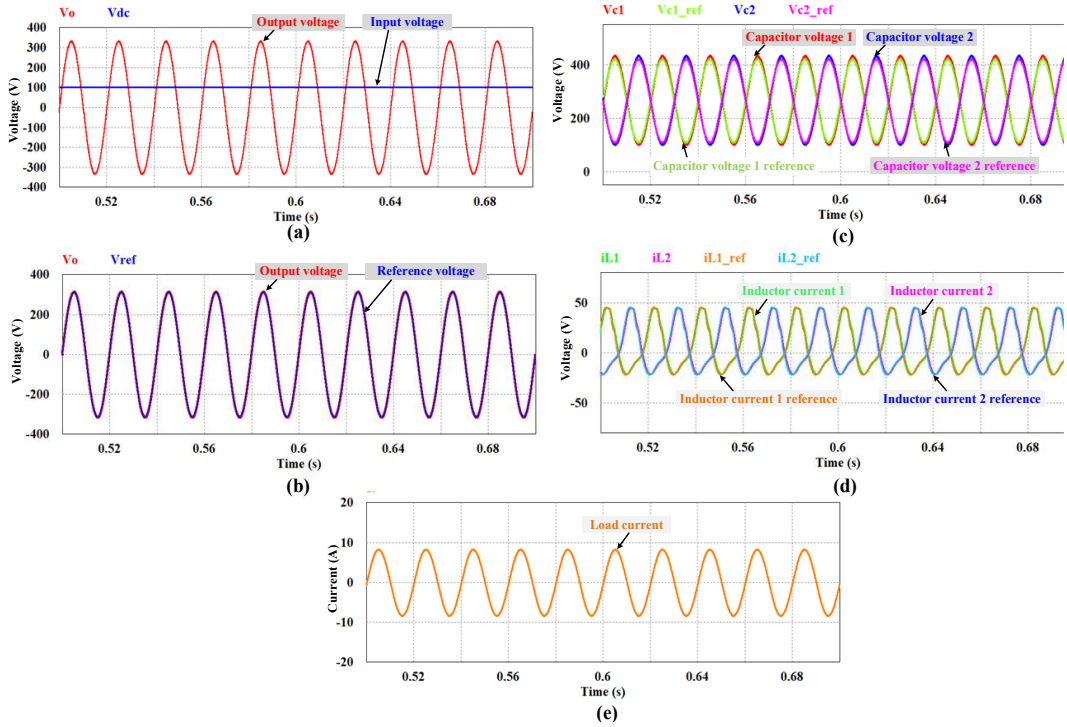

Fig. 6. Simulation results at steady state. (a) Input and output voltages. (b) Output and reference voltages. (c) Capacitor voltages. (d) Inductor currents. (e) Load currents.

Fig. 6(a) illustrates the DC input voltage and the AC output voltage of the inverter under steady-state conditions. While the DC input voltage is maintained at 100 V, the output voltage exhibits a sinusoidal waveform with a significantly higher amplitude, demonstrating the voltage-boosting capability of the differential boost structure. Fig. 6(b) compares the actual output voltage with the reference voltage, showing that the output voltage closely tracks the reference in both amplitude and phase, which confirms the effective operation of the voltage control loop under steady-state conditions. Fig. 6(c) presents the voltages across the two boost capacitors. The capacitor voltages are symmetrical and phase-shifted by 180°, while their average DC levels remain nearly identical. Consequently, the differential voltage between the two capacitors forms a sinusoidal AC output voltage. Fig. 6(d) shows the inductor currents of the two branches, which exhibit near-sinusoidal waveforms and closely follow their reference values, indicating that the current control loop ensures balanced power distribution between the two branches. Fig. 6(e) depicts the output load current, which is sinusoidal and nearly in phase with the output voltage, consistent with the resistive load characteristic and indicating a power factor close to unity.

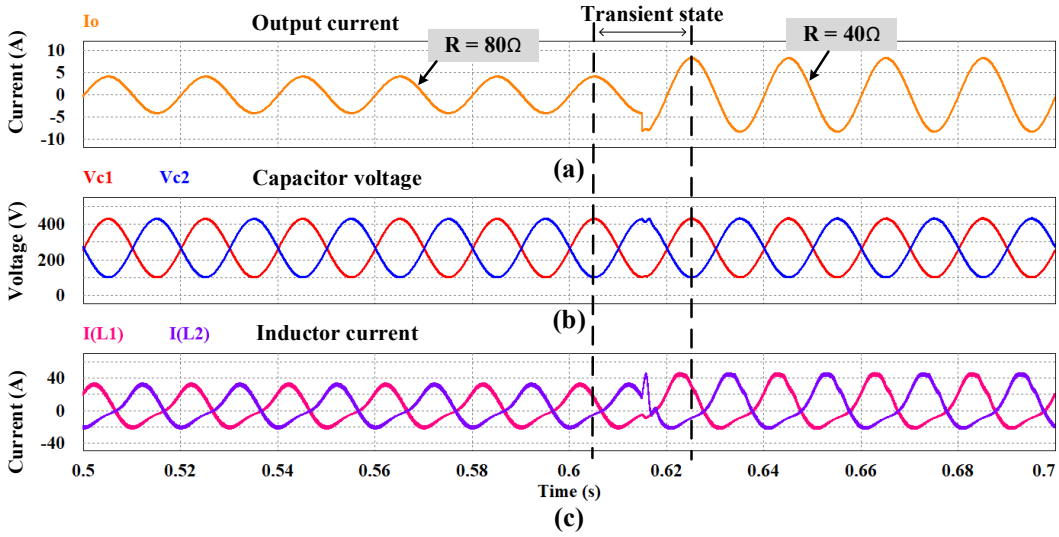

Fig. 7. Simulation results at load change. (a) Output current. (b) Capacitor voltages. (c) Inductor currents.

4.2. Dynamic Response to Load Variations

Fig. 7(a) illustrates the load current when the load resistance is abruptly changed from 80 Ω to 40 Ω. At the instant of the load transition, the current amplitude increases rapidly due to the increased power demand. Following a brief transient period, the load current settles into a steady sinusoidal waveform. Fig. 7(b) presents the capacitor voltages during the load change. When the load increases, a slight drop in the capacitor voltages is observed as more energy is drawn from the system. However, due to the action of the voltage controller, the capacitor voltages are quickly restored to their nominal values while maintaining voltage balance between the two branches. Fig. 7(c) shows the inductor currents during the load transition. Although short-duration transient oscillations occur, the inductor currents rapidly stabilize and continue to track their reference values, indicating that the system exhibits good dynamic response to load variations.

Fig. 8 shows the system response when the DC input voltage varies from 90 V to 110 V. Despite the input voltage change, the output voltage remains stable and closely follows the reference with only minor transient deviations. This result confirms the robustness of the proposed control strategy against input voltage variations.

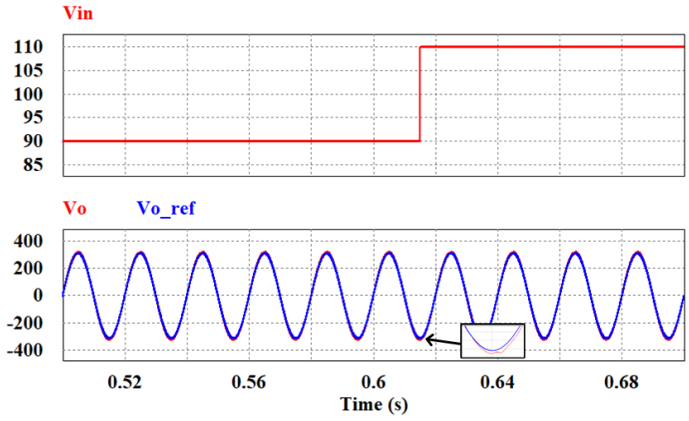

Fig. 8. Output voltage response under input voltage variation (Vin changes from 90 V to 110 V).

5. EXPERIMENTAL RESULTS

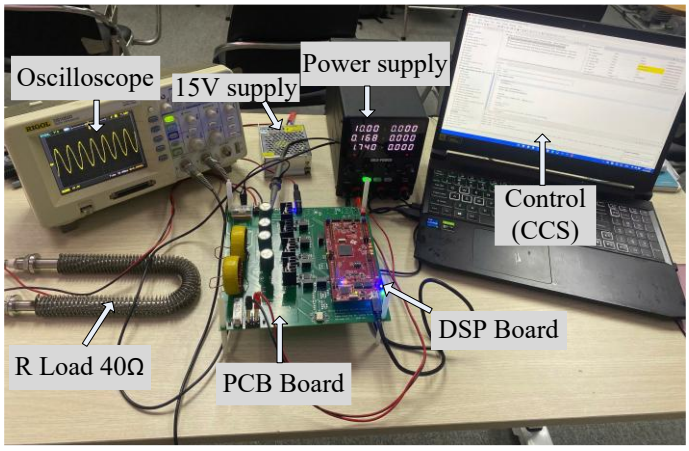

Fig. 9. Experimental setup of the differential boost inverter prototype.

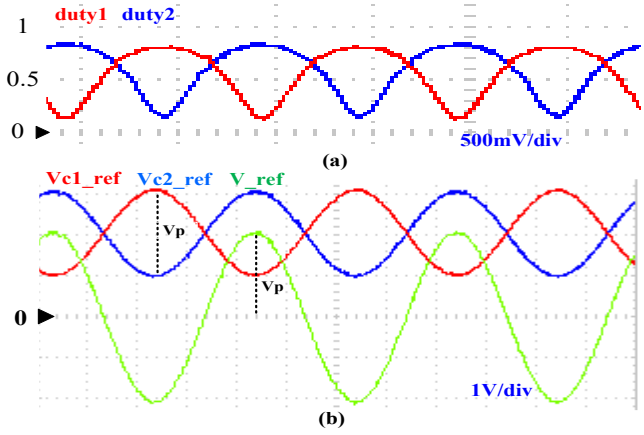

Fig. 10. Reference signal generate by DSP. (a) duty cycles. (b) V_{ref} and V_{C1_ref}, V_{C2_ref}

The laboratory setup of the differential boost inverter prototype is shown in Fig. 9. The system comprises an adjustable DC power supply serving as the input source, a 15 V auxiliary supply for the gate drivers and control circuits, and a power PCB integrating the power semiconductor devices and capacitors. The control algorithm is implemented on a TMS320F28379D DSP control board, while a 40 Ω resistive load is connected at the output terminals. A laptop running Code Composer Studio (CCS) is used to program the DSP and monitor system variables during operation, and the voltage and current waveforms are measured and recorded using a digital oscilloscope.

The main control signals of the system include the reference voltage V_{ref}, the duty cycles, and the PWM pulses generated by the DSP. As shown in Fig. 10(b), the sinusoidal reference voltage V_{ref} and the capacitor reference voltages $V_{C1,\text{ref}}$ and $V_{C2,\text{ref}}$ are generated in the microcontroller at 50 Hz, with the reference amplitude selected according to the desired output voltage level.

Table 2. Input and output voltage levels

DC Input voltage	AC Output voltage RMS
10 V	20 V
20 V	40 V
50 V	80 V
70 V	110 V

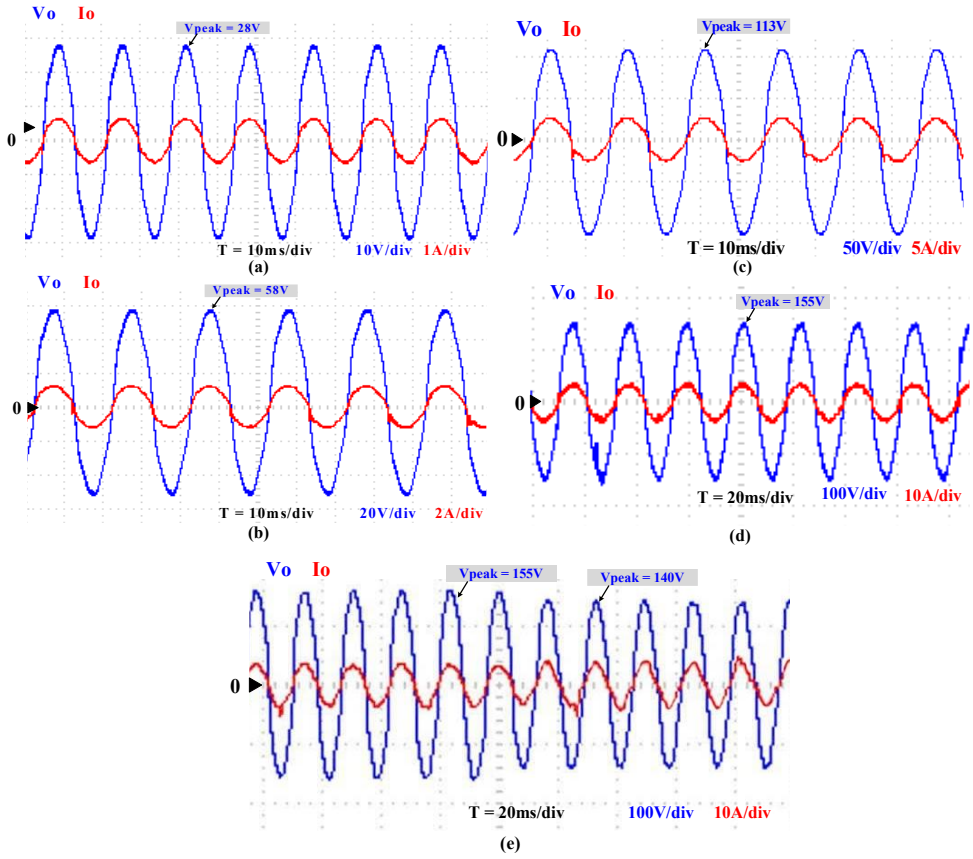

Fig. 11. Experimental results at different input and output voltage levels.
(a) V_{in} = 10V. (b) V_{in} = 20V. (c) V_{in} = 50V. (d) V_{in} = 70V.
(e) Dynamic response of the inverter under load change.

Fig. 10(a) shows the duty cycle waveforms of the two inverter legs, which vary continuously with a sinusoidal envelope following the reference signal. The duty cycles remain within a bounded range and do not reach 0 or 1, indicating that the converter operates in the normal modulation region without saturation.

To evaluate the inverter's voltage amplitude adjustment capability, the system was operated with different input and output voltage levels as shown in Table 2, maintaining the same 40 Ω resistive load throughout the tests.

The experimental results shown in Fig. 11 indicate that the output voltage and current of the inverter increase almost proportionally as the input voltage is raised from 10 V to 70 V. Specifically, at $V_{in} = 10\text{V}$ in Fig. 11(a), the output voltage reaches approximately 20 V RMS; when $V_{in} = 20\text{V}$ in Fig. 11(b), the output voltage increases to about 40 V RMS. As the input voltage is further increased to 50 V in Fig. 11(c), the output voltage reaches approximately 80 V RMS, and at $V_{in} = 70\text{V}$ in Fig. 11(d), the output voltage attains about 110 V RMS. In all

cases, the output voltage waveform remains nearly sinusoidal, and the current load is almost in phase with the voltage, as expected for a resistive load. Although minor switching-related ripples appear at higher power levels, the overall waveform quality remains acceptable, confirming stable operation over the investigated input voltage range.

Another test case was conducted under load increase conditions, where the load resistance was reduced from 40 Ω to 30 Ω. Due to the absence of a feedback mechanism in the open-loop control scheme, the system is unable to regulate the output voltage, resulting in a noticeable voltage drop. As shown in Fig. 11(e), when the load becomes heavier, the current drawn by the load increases to meet the higher power demand. Consequently, a reduction in output voltage accompanied by an increase in load current is observed. This behavior reflects the typical response of an open-loop boost inverter when subjected to load variations.

6. CONCLUSIONS

This paper presents an output voltage control strategy for a single-phase differential boost inverter supplied by a low-voltage DC source and implemented on a TMS320F28379D microcontroller. The proposed topology integrates voltage boosting and AC generation in a single stage, reducing system complexity compared to conventional two-stage structures. A closed-loop control strategy based on PI regulators and an approximate inverse boost compensation block was developed and validated through simulations at the kilowatt level, showing good reference tracking and voltage balance. A low-power prototype using open-loop control was also experimentally tested, confirming the feasibility of the approach, although validation was limited to resistive loads and low-power conditions. Further work will focus on comprehensive experimental evaluation of the closed-loop system under various operating scenarios.

It is feasible to extend the proposed converter to a higher power range of 5–10 kW. However, such an implementation would require the use of higher-rated semiconductor devices, such as SiC MOSFETs or IGBTs, to handle increased electrical stresses. Moreover, additional design considerations, including thermal management, switching loss reduction, and electromagnetic interference mitigation, become more critical at higher power levels. In practice, the adoption of closed-loop control strategies may also be necessary to maintain stable operation and ensure consistent output performance under varying load conditions.

Acknowledgment: This study is funded by the Can Tho University, Code: T2023-111 and THS2025-41.

REFERENCES

[1] S. B. Kjaer, J. K. Pedersen, and F. Blaabjerg, “A review of single-phase grid-connected inverters for photovoltaic modules,” *IEEE Trans. Ind. Appl.*, vol. 41, no. 5, pp. 1292–1306, Sep. 2005, doi: https://doi.org/10.1109/TIA.2005.853371.

[2] Q. Li and P. Wolfs, “A review of the Single Phase photovoltaic module integrated converter topologies with three different DC link configurations,” *IEEE Trans. Power Electron.*, vol. 23, no. 3, pp. 1320–1333, May 2008, doi: https://doi.org/10.1109/TPEL.2008.920883.

[3] Y. Huang, M. Shen, F. Z. Peng, and J. Wang, “Z-source inverter for residential photovoltaic systems,” *IEEE Trans. Power Electron.*, vol. 21, no. 6, pp. 1776–1782, Nov. 2006, doi: https://doi.org/10.1109/TPEL.2006.882913.

[4] P. C. Loh, D. M. Vilathgamuwa, Y. S. Lai, G. T. Chua, and Y. Li, "Pulse-width modulation of Z-source inverters," *IEEE Trans. Power Electron.*, vol. 20, no. 6, pp. 1346–1355, Nov. 2005, doi: https://doi.org/10.1109/TPEL.2005.857543.

[5] F. Gao, P. C. Loh, F. Blaabjerg, and D. M. Vilathgamuwa, "Dual Z-source inverter with three-level reduced common-mode switching," *IEEE Trans. Ind. Appl.*, vol. 43, no. 6, pp. 1597–1608, Nov./Dec. 2007, doi: https://doi.org/10.1109/TIA.2007.908173.

[6] Z. Deng, H. Qin, W. Zhu, Q. Qiu, Y. Deng, and X. He, "Flexible common-mode voltage modulation strategy for differential boost inverters," *Energies*, vol. 17, no. 16, Art. no. 3891, Aug. 2024, doi: https://doi.org/10.3390/en17163891.

[7] Md. Rasheduzzaman, P. Fajri, J. Kimball, and B. Deken, "Modeling, analysis, and control design of a single-stage boost inverter," *Energies*, vol. 14, no. 14, Art. no. 4098, Jul. 2021, doi: https://doi.org/10.3390/en14144098.

[8] B. Hauke, "Basic calculation of a boost converter's power stage," Dec. 2009. Accessed: Sep. 15, 2025. [Online]. Available: https://www.ti.com/lit/an/slva372d/slva372d.pdf

[9] H. V. Nguyen, D. Park, and D. Lee, "Single-phase transformerless PV power conditioning systems with low leakage current and active power decoupling capability," *J. Power Electron.*, vol. 18, no. 4, pp. 997–1006, Jul. 2018, doi: https://doi.org/10.6113/JPE.2018.18.4.997.